



**HAL**  
open science

# Controlled Incorporation of Silver Nanoparticles into Layer-by-Layer Polymer Films for Reusable Electronic Tongues

Rafael C Hensel, Maria L Braunger, Bruno Oliveira, Flavio M Shimizu, Osvaldo N Oliveira, Matthias Hillenkamp, Antonio Riul, Varlei Rodrigues

► **To cite this version:**

Rafael C Hensel, Maria L Braunger, Bruno Oliveira, Flavio M Shimizu, Osvaldo N Oliveira, et al.. Controlled Incorporation of Silver Nanoparticles into Layer-by-Layer Polymer Films for Reusable Electronic Tongues. ACS Applied Nano Materials, 2021, 4 (12), pp.14231-14240. 10.1021/ac-sanm.1c03797 . hal-03526836

**HAL Id: hal-03526836**

**<https://hal.science/hal-03526836v1>**

Submitted on 14 Jan 2022

**HAL** is a multi-disciplinary open access archive for the deposit and dissemination of scientific research documents, whether they are published or not. The documents may come from teaching and research institutions in France or abroad, or from public or private research centers.

L'archive ouverte pluridisciplinaire **HAL**, est destinée au dépôt et à la diffusion de documents scientifiques de niveau recherche, publiés ou non, émanant des établissements d'enseignement et de recherche français ou étrangers, des laboratoires publics ou privés.

# Controlled incorporation of silver nanoparticles into layer-by-layer polymer films for reusable electronic tongues

Rafael C. Hensel,<sup>†</sup> Maria L. Braunger,<sup>†</sup> Bruno Oliveira,<sup>†</sup> Flavio M. Shimizu,<sup>†</sup>  
Osvaldo N. Oliveira Jr.,<sup>‡</sup> Matthias Hillenkamp,<sup>¶,†</sup> Antonio Riul Jr.,<sup>†</sup> and Varlei  
Rodrigues<sup>\*,†</sup>

<sup>†</sup>*Department of Applied Physics, “Gleb Wataghin” Institute of Physics (IFGW), University  
of Campinas (UNICAMP), Campinas, SP 13083-859, Brazil*

<sup>‡</sup>*São Carlos Institute of Physics, University of São Paulo, P.O Box 369, 13560-970 São  
Carlos, SP, Brazil*

<sup>¶</sup>*Institute of Light and Matter, University of Lyon, University Claude Bernard Lyon 1,  
CNRS, UMR5306, F-69622 Villeurbanne, France.*

E-mail: varlei@ifi.unicamp.br

## Abstract

The incorporation of metallic nanoparticles in sensors and biosensors normally enhances performance, but fabricating reproducible sensing units is still an issue owing to the poor control of their electrical properties. In this article, we exploit the controlled deposition of silver nanoparticles (NP) pre-formed in a gas phase into layer-by-layer (LbL) films of poly(allylamine hydrochloride) (PAH) and poly(sodium 4-styrenesulfonate) (PSS) (PAH/PSS) assembled on gold interdigitated electrodes (IDEs). *In-situ* impedance measurements during NP deposition permitted the monitoring of the electrical response evolution, and reproducible sensing units could be made with tailored characteristics by varying the deposition time. In proof-of-principle experiments we employed an array with 4 sensing units in an electronic tongue (e-tongue), which was capable of distinguishing basic flavors of the human palate and diverse commercial umami-based flavor enhancer. Using statistical analysis methods it was possible to identify ways to optimize the e-tongue performance, thus confirming the possibility to explore controlled changes in electrical response via nanoparticle incorporation. It is worth noting that the methodology can be extended to produce other polymer-metallic NP composites and modify the electrical behavior of films in a controlled, reproducible manner, opening the way for enhanced opto-electronic devices, not limited to sensors or biosensors.

## Introduction

The development of sensors for efficient, rapid, and reliable **detection of analytes in volatile compounds or complex liquids** is a global demand for environmental, agricultural, and food monitoring. A promising approach to the fabrication of sensing devices is to exploit nanostructured polymers as active layers to tune physicochemical properties with high precision,<sup>1</sup> and/or dope the polymer matrix to enhance sensing performance. For instance, the incorporation of metallic aggregates in polymeric matrices enhances sensing via the optical and electrical response due to the high surface-to-volume ratio of nanoparticles.<sup>2</sup> By

28 way of illustration, functionalization of glassy carbon electrodes with ferrocene terminated  
29 poly(amidoamine) dendrimers encapsulated with gold nanoparticles promoted high sensitiv-  
30 ity and stability in detecting 4-aminophenol,<sup>3</sup> and cobalt phthalocyanine films modified with  
31 palladium and gold nanoparticles improved the performance of chemiresistive sensors for hy-  
32 drogen.<sup>4</sup> In these examples, the enhancement mechanism can be related to the functional  
33 groups of the coating, to an increase in the surface area, modifications of the conductive  
34 path and geometric parameters.<sup>2,5</sup> Incorporation of metallic nanoparticles in sensors can  
35 enhance their specificity,<sup>6</sup> sensitivity,<sup>7</sup> and selectivity,<sup>8-12</sup> but an independent control of the  
36 nanoparticle synthesis and deposition to fine-tune the device response is still a technological  
37 bottleneck. With wet chemistry one may synthesize nanoparticles protected with functional  
38 groups that interact specifically with the analyte to increase selectivity,<sup>13</sup> and the thickness  
39 of the functional layer can be adjusted to favor the nanoparticle spatial ordering.<sup>14</sup> The  
40 synthesis and deposition of nanoparticles may also be carried out with atomic deposition  
41 of evaporated and/or sputtered metallic particles.<sup>13</sup> However, this method is limited since  
42 the wettability and mobility of atoms on the surface promote coalescence of the nanoparti-  
43 cles,<sup>15-19</sup> making it difficult to control their size and spatial distribution. To overcome these  
44 limitations one can deposit nanoparticles produced in the gas phase.<sup>20,21</sup> In this method,  
45 atoms sputtered from a metallic target<sup>21</sup> aggregate in an inert gas atmosphere under defined  
46 pressure and temperature. Then the pre-formed nanoparticles can be deposited at a defined  
47 kinetic energy to maintain their structure. The advantage of this technique is in the con-  
48 trol of nanoparticle size, maintaining the nanoparticle interface free from surfactants. The  
49 fundamental differences between sputtered and passivated chemically synthesized nanopar-  
50 ticles are significant since plasmonic properties, chemical reactivity, catalytic activity, and  
51 electrical conduction critically depend on the particle-environment interface.

52 Here we explored the versatility of gas-phase generated nanoparticles to adjust in a con-  
53 trolled way the electrical response of a layer-by-layer film of poly(allylamine hydrochloride  
54 (PAH) and poly(sodium 4-styrene sulfonate) (PSS). In addition to the independent control

55 over the nanoparticle composition and size, as the deposition is performed in vacuum, the  
56 nanoparticles are free from surfactants and passivation layers. The electrical behavior of  
57 PAH/PSS films on interdigitated electrodes (IDEs) was monitored during the deposition of  
58 silver nanoparticles by impedance measurements. This method allowed us to tune the elec-  
59 trical behavior of PAH/PSS films with high reproducibility according to device impedance,  
60 and employ them in sensing units for an electronic tongue (e-tongue). Many types of ma-  
61 terials have been used in nanostructured films for e-tongues,<sup>22-25</sup> which are based on the  
62 global selectivity principle,<sup>26,27</sup> according to which the electrical responses of an array of  
63 sensing units are combined to establish a "fingerprint" of the liquid under analysis. For  
64 some applications of e-tongues, however, the choice of materials and sensing units must be  
65 judicious to permit them to be reused. The two most stringent requirements for reuse are  
66 reproducibility of the electrical response and robustness against contamination. We show  
67 here that sensing units made with nanoparticle-containing PAH/PSS films fulfill these re-  
68 quirements in proof-of-principle experiments with e-tongues capable of distinguishing the  
69 basic tastes and different food samples with umami taste.

## 70 **Methodology**

### 71 **Polymeric thin films**

72 Gold IDEs on glass with 30 pairs of digits with 3 mm length, 200 nm height, 40  $\mu\text{m}$  width,  
73 and spaced 40  $\mu\text{m}$  from each other, were fabricated at the National Center for Research in  
74 Energy and Materials (CNPEM) Brazil. To favor adsorption of the polymer film on the  
75 IDE, we executed a cleaning procedure using a solution of hydrogen peroxide, ammonium  
76 hydroxide, and deionized water in the proportion (1:1:5). The IDE stood immersed for  
77 10 min at a fixed temperature around 80°C. The polymeric thin films were deposited onto  
78 IDEs using the layer-by-layer (LbL) method<sup>28,29</sup> with alternating layers of PAH and PSS  
79 purchased from Sigma-Aldrich and used as received. The PAH and PSS solutions had 0.5

80 mg/mL in deionized water acquired from an Arium Comfort Sartorius system, whose pH was  
 81 adjusted to 7. The LbL films were fabricated using a homemade automated setup, described  
 82 elsewhere.<sup>30</sup> We set the immersion time for both PSS and PAH to 8 min, with a 10 mm/min  
 83 withdrawal speed. Although PAH and PSS are polyelectrolytes, the electrostatic interactions  
 84 during the multilayer assemble promotes the formation of electrical dipoles, which confer an  
 85 insulating behavior for the PAH/PSS LbL architecture.<sup>31</sup>

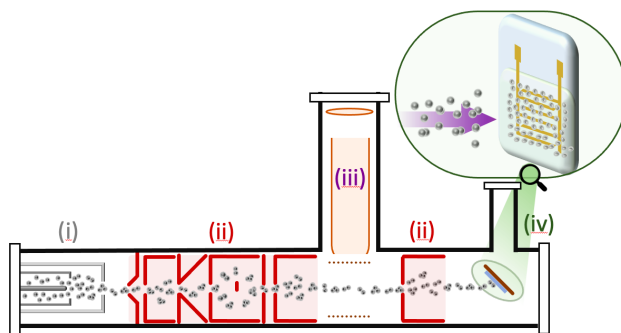


Figure 1: Schematic illustration of the experimental setup. Atomic cluster source used to produce and deposit the silver nanoparticles in the LbL film: (i) magnetron sputtering; (ii) set of electrostatic lens; (iii) time of flight mass spectrometer (TOF-MS); (iv) deposition chamber.

## 86 Nanoparticle production and deposition

87 Nanoparticles were produced in the gas phase using a gas-aggregation source shown in Fig-  
 88 ure 1.<sup>32</sup> Metal atoms are sputtered from a wire target. In a buffer gas (He/Ar), the atomic  
 89 collisions and quenching cause nanoparticle formation (Figure 1(i)). A major fraction of the  
 90 nanoparticles is positively charged and is guided through vacuum by a set of electrostatic  
 91 lenses (Figure 1(ii)). Neutral nanoparticles are removed from the beam using a barrier. To  
 92 monitor the nanoparticle size during deposition, a small fraction of the charged nanoparticles  
 93 is deflected towards a TOF-MS, indicated in Figure 1(iii). The main nanoparticle beam is  
 94 guided to the sample holder, where deposition occurs (Figure 1(iv)). The nanoparticle flux  
 95 is monitored with a Keithley Series 6487 Picoammeter. We deposited silver nanoparticles  
 96 of average diameter of 3 nm, with a typical current of 300-500 pA measured on the current

97 detector with  $75 \text{ mm}^2$  area. The IDE electrical response was monitored during the silver  
98 nanoparticle deposition *in situ* using a homemade impedance meter, described in detail else-  
99 where.<sup>33</sup> Briefly, a sinusoidal voltage of 1 V amplitude and 1 kHz is applied to one comb of the  
100 IDE digits. The current from the pick-up electrode is amplified using an operational amplifier  
101 in a differential configuration.<sup>30</sup> A lock-in system measures the output voltage and the phase  
102 shift between the input and output signals. We interpreted the impedance measurements  
103 using an equivalent circuit coupling parallel capacitive and conductive components.<sup>30</sup>

## 104 **Impedance spectroscopy**

105 The electrical response of the IDEs in distilled water was evaluated using an impedance  
106 analyzer Solartron 1260A coupled to a dielectric interface model 1296A. The input voltage  
107 amplitude was set to 25 mV, with impedance measurements taken in the frequency range  
108 1 Hz -  $10^6$  Hz, and interpreted using an equivalent electrical circuit of resistors and capaci-  
109 tors. We repeated this measurement after the PAH/PSS film assembly, and then nanoparticle  
110 deposition.

## 111 **Morphological investigation**

112 Two LbL films were prepared with different concentrations of silver nanoparticles incor-  
113 porated in the PAH/PSS to investigate the depth profile of the silver nanoparticles in the  
114 polymer matrix. Using a Dual Beam Helios 660 from the CNPEM, we produced sample cross-  
115 section lamellae with the lift-off method<sup>34</sup> which were analyzed using Scanning Transmission  
116 Electron Microscopy with a High Angle Annular Dark Field (STEM-HAADF) detector in a  
117 JEOL 2100F operated at 200 kV, also from CNPEM.

## 118 E-tongue measurements

119 In proof-of-principle experiments, we employed an impedimetric electronic tongue (e-tongue)  
120 comprising sensing units of IDEs coated with PAH/PSS films with incorporated nanopar-  
121 ticles. The combination of several sensing units in an e-tongue aims at obtaining distinct  
122 electrical behaviors to provide a unique **fingerprint** of the samples.<sup>35</sup> To achieve this, we  
123 defined a procedure similar to the one reported by Garçon *et al*, in which they varied the  
124 proportion of two building blocks to differentiate the sensing units.<sup>36</sup> We used **one** bare IDE  
125 and **three** IDEs covered with 150-bilayer (PAH/PSS) LbL films, two of which had different  
126 concentrations of deposited silver nanoparticles. From here on, the sensing units will be  
127 referred to as follows: IDE 1 is the bare IDE, IDE 2 is covered by 150 PAH/PSS bilayers,  
128 IDEs 3 and 4 were the coated with 150-bilayer PAH/PSS LbL films with a lower and a  
129 higher concentration of silver nanoparticles, respectively. We chose silver nanoparticles for  
130 the efficient and easy production control in the atomic cluster source. The e-tongue per-  
131 formance was evaluated in basic tastes relevant to the human palate. We prepared 1 mM  
132 aqueous solutions of caffeine ( $C_8H_{10}N_4O_2$ ), sucrose ( $C_{12}H_{22}O_{11}$ ), sodium chloride (NaCl), hy-  
133 drochloric acid (HCl), and L-glutamic acid ( $C_5H_9NO_4$ ), corresponding respectively to bitter,  
134 sweet, salty, sour, and umami tastes. The measurements were performed in triplicate using  
135 a Solartron 1260A coupled to a dielectric interface model 1296A in the same configuration  
136 described before. **The analysis were performed by immersing each IDE in a Becker contain-**  
137 **ing the analyte solution in the following order: sucrose, caffeine, L-glutamic acid, NaCl, and**  
138 **HCl.** We verified all sensing units in water after measuring **each analyte** sample to check  
139 possible cross-contamination caused by the analytes in the sensing units.

140 As a further test of the sensor selectivity, we analyzed samples that give umami fla-  
141 vor to food. These samples were provided by the Food Ingredients Division of Ajinomoto  
142 in Brazil, comprising monosodium glutamate (Aji-no-moto<sup>®</sup>), disodium inosinate (Ajitide  
143 IMP<sup>®</sup>), disodium inosinate + disodium guanylate in 1:1 ratio (Ajitide I+G<sup>®</sup>), and a yeast  
144 extract with umami flavor (Savorboost U<sup>®</sup>), in addition to a commercial monosodium

145 glutamate sample purchased in the United States of America (Accent<sup>®</sup>). Except for Sa-  
146 vorboost U<sup>®</sup>, the chemical formulas of these umami samples differ from each other by a  
147 few atoms: Aji-no-moto<sup>®</sup> (C<sub>5</sub>H<sub>8</sub>NNaO<sub>4</sub>), Ajitide IMP<sup>®</sup> (C<sub>10</sub>H<sub>11</sub>N<sub>4</sub>Na<sub>2</sub>O<sub>8</sub>P), Ajitide I+G<sup>®</sup>  
148 (C<sub>10</sub>H<sub>11</sub>N<sub>4</sub>Na<sub>2</sub>O<sub>8</sub>P + C<sub>10</sub>H<sub>12</sub>N<sub>5</sub>Na<sub>2</sub>O<sub>8</sub>P). In addition, Aji-no-moto<sup>®</sup> and Accent<sup>®</sup> are com-  
149 posed of monosodium glutamate provided by different manufacturer. All measurements were  
150 compared to L-glutamic acid, with 2 mg of each analyte dispersed in 1 mL distilled water.  
151 The measurements were also performed by immersing the IDEs in each analyte solution in  
152 the following order: Aji-no-moto<sup>®</sup>, Accent<sup>®</sup>, L-glutamic acid, Ajitide IMP<sup>®</sup>, Ajitide I+G<sup>®</sup>,  
153 and Savorboost U<sup>®</sup>, also cross-checking the measurement in water after each analyte anal-  
154 ysis.

## 155 Results and discussion

### 156 Electrical characterization

157 The controlled incorporation of silver nanoparticles in the PAH/PSS films was evaluated with  
158 *in-situ* impedance measurements performed at 1 kHz. Figure 2 shows that IDE 3 and IDE  
159 4 had an impedance  $8 \times 10^8 \Omega$  before the nanoparticle incorporation started, indicating the  
160 insulating behavior of the polymer matrix. The impedance of these electrodes decreased only  
161 slightly during the first 0.6 h deposition at a rate of  $-0.6 \times 10^8 \Omega/h$ , after which it dropped  
162 considerably. When nanoparticle incorporation was interrupted for IDE 3, after 1.4 h of  
163 deposition ( $\sim 0.7$  AgNP monolayer), its impedance stabilized at  $1.0 \times 10^8 \Omega$ . Incorporation  
164 continued for IDE 4 until almost two hours ( $\sim 0.9$  AgNP monolayer), which caused the  
165 impedance to decrease further and stabilize at  $1.2 \times 10^7 \Omega$ . It is worth noting that the  
166 impedance response is nearly identical for IDE 3 and IDE 4 before stopping deposition  
167 on IDE 3. Overall, in addition to indicating that the sensing units can be differentiated  
168 according to their impedance, the reproducibility of nanoparticle incorporation (Figure S1  
169 in the Supporting Information) permits to fabricate devices with an adjustable electrical

170 response.

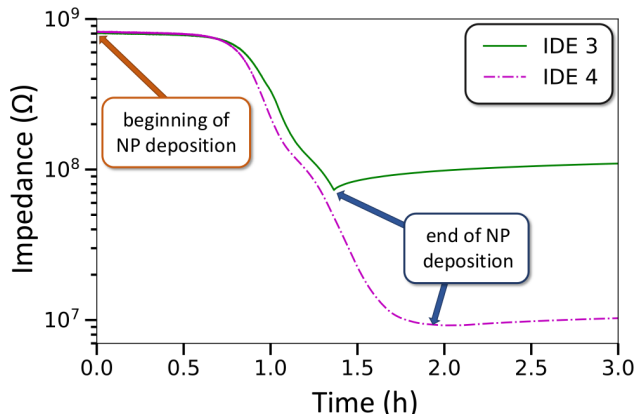


Figure 2: Impedance measurement at 1 kHz as a function of time of incorporation of silver nanoparticles for IDE 3 and IDE 4, with dashed lines marking the interruption of the incorporation. IDE 3 and IDE 4 had 150-bilayer PAH/PSS LbL films.

171 The electrical properties of the four sensing units with IDEs described in the method-  
172 ology were assessed through impedance measurements in distilled water. The Nyquist plot  
173 in Figure 3(a) shows a semicircle corresponding to  $10\text{ k}\Omega$  followed by a diffusion process for  
174 the bare electrode (IDE 1). The deposition of a PAH/PSS LbL film onto IDE 2 caused the  
175 emergence of a second semicircle, the diameter of which further increased with the concen-  
176 tration of deposited silver nanoparticles (IDE 3 and IDE 4). A semicircle in a Nyquist plot is  
177 associated with a parallel coupling of capacitive and resistive components. To investigate the  
178 changes in electrical properties due to surface modification, the impedance data were inter-  
179 preted using equivalent circuits<sup>37</sup> with the ZView software.<sup>38</sup> The fitted curves according to  
180 the equivalent circuits are also plotted as solid lines in Figure 3(a). The circuit that best rep-  
181 resented the data for IDE 1 is shown in Figure 3(b), where  $R_{dl}$  and  $C_{dl}$  are the double-layer  
182 resistance and capacitance, respectively,  $R$  is the resistance after the double-layer formation  
183 which hinders charge mobility, CPE is the constant phase element assigned to an imperfect  
184 capacitance that is due to surface roughness and imperfections, and  $C_g$  is the geometric  
185 capacitance.<sup>37</sup> With deposition of a LbL film on electrodes IDE 2, IDE 3, and IDE 4 and  
186 incorporation of silver nanoparticles (IDE 3, and IDE 4), the equivalent circuit had to be  
187 extended to consider the contribution of the deposited materials onto the IDEs. The parallel

188 association of  $R_f$  and  $C_f$  represents the resistance and capacitance of the deposited material,  
189 respectively, as shown in Figure 3(c). CPE in the circuit of Figure 3(c) takes into account  
190 the surface imperfections due to adsorption of the film and silver nanoparticles deposition.  
191 The parameters used to fit the data with the equivalent circuits are given in Table 1, with  
192 high-quality fitting indicating by a  $\chi^2$  of the order of  $10^{-5}$ . At low frequencies ( $< 100$  Hz)  
193 the electric signal is dominated by double-layer effects, and the resistance  $R_{dl}$  increases from  
194 184 to 214 k $\Omega$  due to the insulating LbL film, which then decreased to 61 and 56 k $\Omega$  with the  
195 increase of the deposited silver nanoparticles. The nanoparticle deposition causes the double  
196 layer capacitance to decrease owing to a reduction on the space between the "plates" of  $C_{dl}$ .  
197 The Bode plot in Figure 3 (d) indicates that the low frequency impedance decreases due to  
198 the polymer matrix and nanoparticles, which can be associated with ion accumulation on  
199 the device interface with the double-layer effects. At intermediate frequencies, dominated by  
200 the interfacial film/electrolyte response, the film resistance decreases with the nanoparticle  
201 deposition. This is attributed to creation of conducting paths in the (PAH/PSS) matrix.<sup>2</sup>  
202 The film capacitance increases with the nanoparticle deposition and their agglomeration in  
203 the polymer matrix. The extreme case here is the formation of a metallic nanoparticle film  
204 that is equivalent to introducing a new capacitor plate that reduces the gap between the  
205 capacitor plates. In the same frequency range, R and CPE increased with deposition of the  
206 LbL films and increasing incorporation of nanoparticles, which is explained by the decrease  
207 of the n factor,<sup>37</sup> thus suggesting a transition, of the whole system, from a capacitance to a  
208 resistance behavior. The Bode plots in Figure 3 (d) corroborate these interpretations, with  
209 an impedance increase in the intermediary frequency range ( $10^2$  Hz and  $10^4$  Hz), where the  
210 electrical response is dominated by the film/electrolyte interface<sup>39</sup>. The dark arrow is a  
211 guide to the eye to illustrate the impedance increase in this frequency range. Note that the  
212 impedance at 1 kHz in Figure 2 decreases with the nanoparticle deposition, in contrast to  
213 the result in Figure 3 (d) because the measurements were performed in distinct media, i.e.  
214 vacuum (Figure 2) and distilled water (Figure 3 (d)). At higher frequencies ( $> 100$  kHz),

215 the response is dominated by the geometry of the electrodes, which is constant, i.e.,  $C_g \approx$   
 216 74 pF.

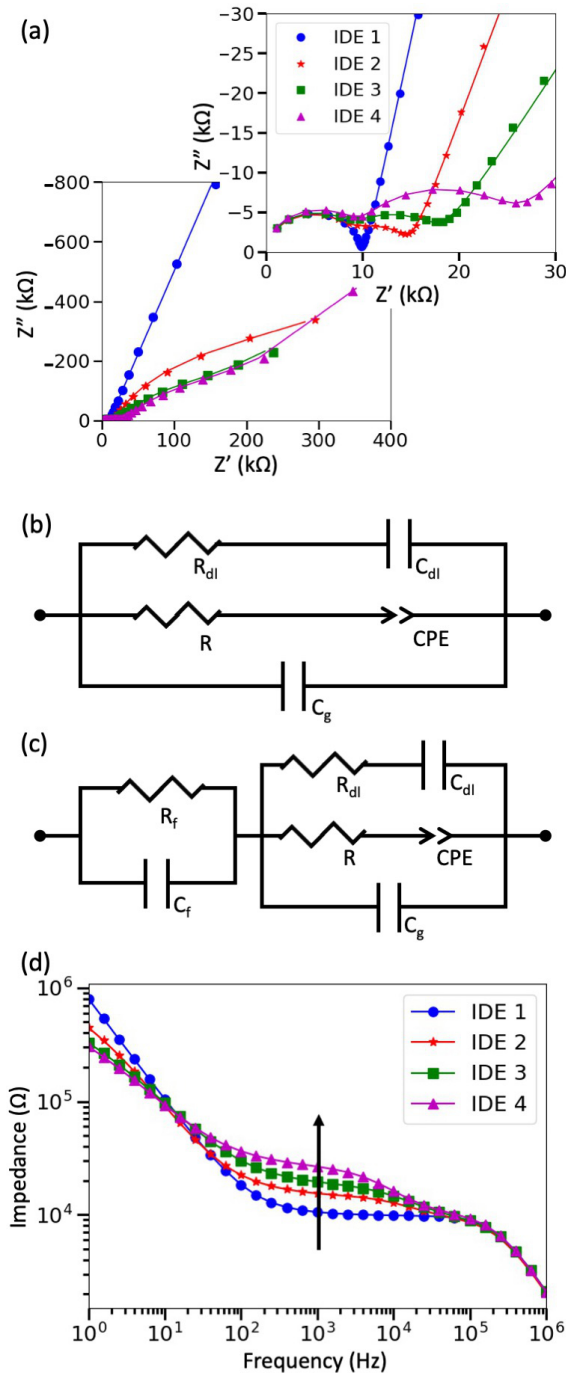


Figure 3: (a) Nyquist plots of IDEs 1-4 in distilled water. The solid lines indicate the fit using equivalent circuit evaluation. Scheme of the equivalent circuit used to evaluate (b) IDE 1, (c) IDE 2, IDE 3, and IDE 4. (d) Bode plots of the IDEs 1-4 in water. The black arrow is a guide to the eye to illustrate the impedance increase of the distinct sensing units.

Table 1: Fitting values for the equivalent circuit elements used to simulate the impedance spectra in Figure 3

IDEs	$R_{dl}$ (k $\Omega$ )	$C_{dl}$ ( $\mu$ F)	$R_f$ (k $\Omega$ )	$C_f$ (nF)	R (k $\Omega$ )	CPE( $\mu$ F)	n	$C_g$ (pF)
IDE 1	184 $\pm$ 9	0.54 $\pm$ 0.06	-	-	10.33 $\pm$ 0.01	0.24 $\pm$ 0.01	0.89 $\pm$ 0.01	73.35 $\pm$ 0.01
IDE 2	214 $\pm$ 7	0.45 $\pm$ 0.01	29.2 $\pm$ 0.3	0.259 $\pm$ 0.006	14.33 $\pm$ 0.04	1.03 $\pm$ 0.03	0.71 $\pm$ 0.01	75.9 $\pm$ 0.3
IDE 3	61 $\pm$ 2	0.66 $\pm$ 0.02	24.4 $\pm$ 0.3	0.274 $\pm$ 0.005	16.77 $\pm$ 0.07	1.23 $\pm$ 0.02	0.61 $\pm$ 0.02	72.7 $\pm$ 0.3
IDE 4	56 $\pm$ 5	0.98 $\pm$ 0.06	19.6 $\pm$ 0.2	0.50 $\pm$ 0.01	24.0 $\pm$ 0.2	1.43 $\pm$ 0.03	0.58 $\pm$ 0.01	74.3 $\pm$ 0.6

217

## 218 Nanoparticle depth profile

219 The depth profile for the nanoparticles incorporated in the (PAH/PSS) polymer matrix  
 220 was determined from the cross-section lamellae using STEM-HAADF. Figure 4 (a) and  
 221 (b) show STEM-HAADF micrographs for samples with low and high silver nanoparticle  
 222 concentrations, similar to IDE 3 and IDE 4, respectively. The sketch in Figure 4 (c) helps  
 223 identify the sample cross-section layers. Carbon and platinum layers were deposited to reduce  
 224 damages during ion beam milling on the polymeric film with nanoparticles. Bright spots  
 225 due to the silver nanoparticles are seen below the carbon layer in Figures 4 (a) and (b). In  
 226 both cases, the micrographs indicate that silver nanoparticles were deposited in the polymer  
 227 matrix, and agglomerated in bigger structures near the polymer surface, especially for the  
 228 high nanoparticle concentration. Although the micrographs do not have enough particles  
 229 for a size distribution analysis, we measured their diameter in the direction perpendicular to  
 230 the substrate (Figure 4), obtaining a mean diameter of 11  $\pm$  6 nm and 19  $\pm$  4 nm for lower  
 231 and higher concentrations, respectively (Figure S2 in the Supporting Information). However,  
 232 we must be careful in estimating the agglomeration size as TEM micrographs are projected  
 233 images, so the measured diameter can be related to more than one projected structure due  
 234 to the non-negligible lamellae thickness.

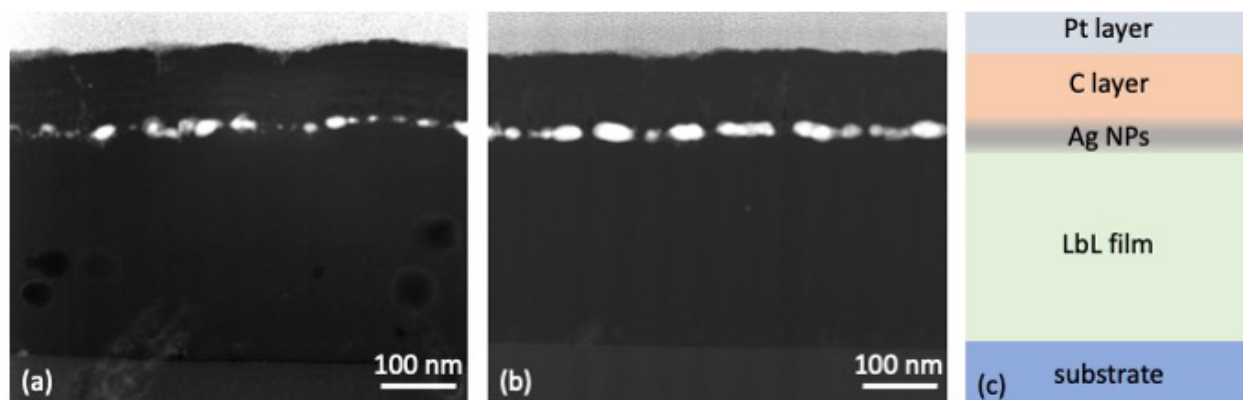


Figure 4: HAADF STEM micrographs of samples with nanoparticle concentrations similar to those of (a) IDE 3, and (b) IDE 4, respectively. (c) Sketch of the samples cross-section's tiers.

### Impedimetric E-tongue

The control of electrical response imparted by incorporation of silver nanoparticles into LbL films was exploited in proof-of-principle experiments with an impedimetric e-tongue made with the four sensors in two tasks: to distinguish among the aqueous solutions representing the basic tastes and differentiate flavor enhancers with umami taste. We first demonstrate that a single sensing unit is already capable of some differentiation of the basic tastes, as indicated in the impedance spectra obtained with IDE 4 in Figure 5 (a). Indeed, in subsidiary statistical analyses we verified that full distinction of the basic tastes was possible with this sensing unit, as will be demonstrated later on. A similar finding was observed for the other three sensing units whose spectra are shown in Figures S2 in the Supporting Information. It is significant in the figure that the spectra for sucrose and caffeine are similar because they are weak electrolytes. Another important issue here is to investigate if the taste solutions change irreversibly the impedance response of the devices. Figure 5 (b) shows that the impedance spectra for IDE 4 in water is not affected by measurements in the basic taste solutions, which means there is no cross-contamination of the sensing unit. We repeated this procedure for IDEs 1-3, and there was no evidence of cross-contamination either, as shown in Figures S3 in the Supporting Information.

We applied principal component analysis (PCA)<sup>40</sup> over the whole impedance spectra to

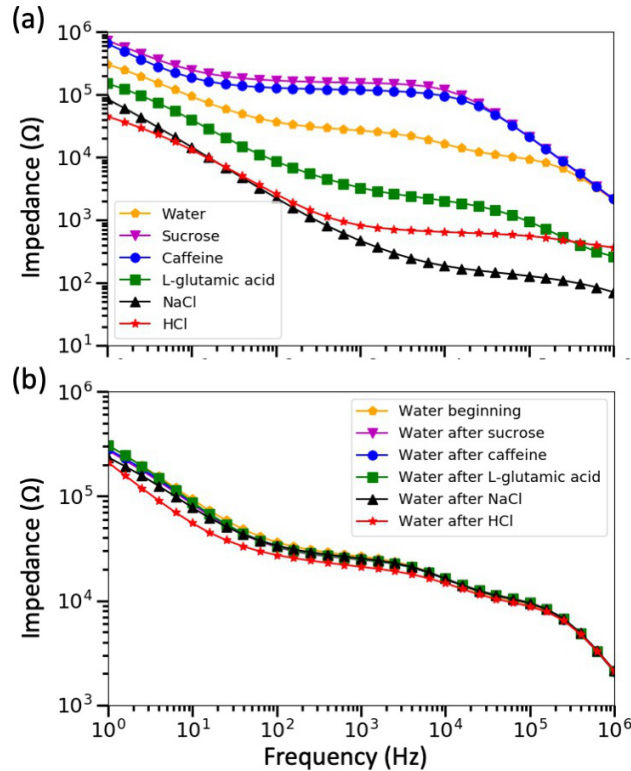


Figure 5: Impedance spectra for IDE 4: (a) in the aqueous solutions corresponding to the basic taste; (b) in water after measurement in the basic taste solutions.

252

253 investigate the capability of each sensing unit of the e-tongue for discriminating the basic fla-  
 254 vor analytes. We used the open-source software Orange for data analysis and visualization,<sup>41</sup>  
 255 which makes it possible to evaluate the number of clusters using the k-means method.<sup>42</sup>  
 256 Briefly, k-means interactively defines the center of each cluster, minimizing the sum of square  
 257 Euclidean distances between the center and its assigned data points. The quality of the clus-  
 258 ter was compared using the silhouette plot, evaluating how close each point in one cluster  
 259 is to points in the neighboring clusters. The silhouette value  $s(i)$  of the  $i^{\text{th}}$  cluster ranges  
 260 between -1 and 1, with the following interpretation: (a) if  $s(i) \sim 1$  the object is well classified  
 261 in a cluster; (b) if  $s(i) \sim 0$  the object lies between two clusters; (c) if  $s(i) \sim -1$  the object  
 262 is badly classified. The maximum value for mean  $\overline{S(k)}$  over all objects in the data set for  $k$   
 263 clusters provides the silhouette coefficient (SC), which varies between 0 and 1 having the fol-  
 264 lowing interpretation: (a)  $0.71 < SC < 1.00$  corresponds to a strong distinction capability;

265 (b)  $0.51 < SC < 0.70$  means a reasonable distinction capability; (c)  $0.26 < SC < 0.50$  refers  
266 to a weak or artificial distinction capability; (d)  $SC \leq 0.25$  corresponds to no distinction  
267 capability at all.<sup>43,44</sup> Figure S5 in the Supporting Information shows that IDE 1, IDE 2, and  
268 IDE 3 can discriminate the basic tastes for the human palate. However, with IDE 4 the data  
269 for one caffeine sample is out of the expected cluster. The mean silhouette of each cluster  
270 for each sensing unit is shown in Table 2. From the SC values we infer that IDE 1 better  
271 distinguishes all analytes, with IDE 3 presenting the second highest SC value and better  
272 discrimination for strong electrolytes (HCl, L-glutamic acid, NaCl), with  $S(k) > 0.91$ . This  
273 indicates that insertion of the nanoparticles into the polymer matrix increases the ability to  
274 identify electrolytes, possibly due to higher interacting area (from nanoparticles) with ions  
275 in solution. Surprisingly, IDE 4 exhibited lower SC compared to IDE 3, maybe because it  
276 poorly recognized caffeine triplicate. Our interpretation is that the high concentration of  
277 silver nanoparticles in IDE 4 was deleterious to the electrical response owing to nanoparti-  
278 cle clustering/compaction during the deposition process. That a single sensing unit could  
279 already provide full distinction of the samples is attributed to the combination of electrical  
280 responses from various frequencies, as different mechanisms govern the electrical response at  
281 distinct frequency regions. Hence, one sensing unit may play the role of an e-tongue if one  
282 considers that global selectivity is warranted by this combination of responses.

283 We also verified that combining the sensing units led to an increase in SC in Table  
284 S1 in the Supporting Information. As expected, a higher SC was obtained combining the  
285 impedance spectra of all sensing units. Results for the five basic tastes with the whole  
286 impedance frequency range for the four sensing units are shown in Figure 6, where each  
287 spectrum is represented by a marker. There are three markers for each analyte because  
288 the measurements were made in triplicate. Table 2 lists the mean silhouette value  $\overline{s(i)}$  for  
289 each cluster  $i$  in the set of  $k$  clusters in Figures 6, with the highest silhouette coefficients  
290 (SC) obtained using the k-means method.  $\overline{s(k)} = 0.88$  for a classification in  $k=5$  clusters.  
291 According to Figure 6 and Table 2 the main difference in electrical response captured by the e-

292 tongue can be established with only the first principal component (PC1) that describes 99.0%  
 293 of the data. Thus PC1 distinguishes electrolytes (HCl, NaCl, and L-glutamic acid, in the  
 294 left-hand side) from non-electrolytes (caffeine and sucrose, in the right hand side). Although  
 295 the second principal component (PC2) expresses only 0.5%, it is capable of distinguishing  
 296 the three electrolyte samples, and the two non-electrolyte samples. It is worth noting that  
 297  $\overline{s(i)} > 0.71$  in all cases owing to a strong distinction capability for the data in each cluster  $i$ .  
 298 Of special relevance was the separation of the umami flavor (L-glutamic acid) in Figure 6,  
 299 which is an achievement since this flavor is difficult to distinguish using e-tongues.<sup>25,45</sup>

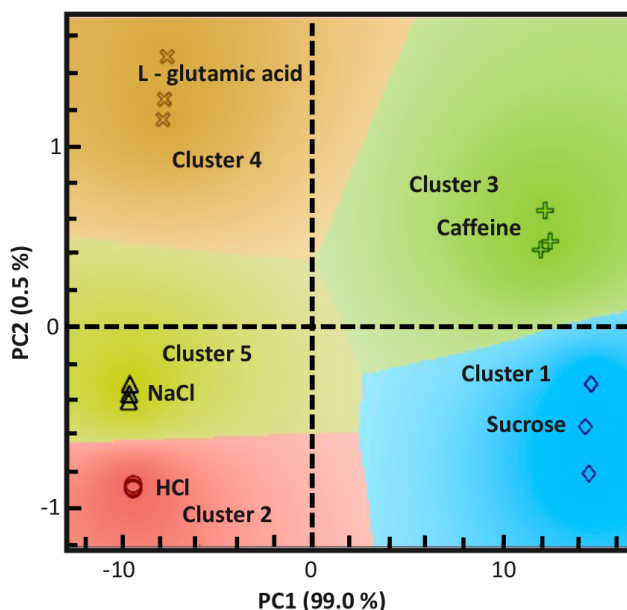


Figure 6: PCA plot with the impedance spectra obtained with the electronic tongue for the basic flavors: HCl (sour), L-glutamic acid (umami), NaCl (salt), caffeine (bitter), sucrose (sweet). The data set was separated into five clusters according to the maximum  $\overline{S(k)}$  value that correctly distinguished the five samples.

300

301 The positive results for umami in the evaluation of the basic tastes motivated us to pursue  
 302 it further in samples of food enhancers. This topic has deserved increasing attention owing  
 303 to the difficulties with the umami flavor, for which e-tongues have been produced with  
 304 various materials, including peptides, biotaste receptors and polymers with nanoparticles  
 305 incorporated.<sup>46-55</sup> Figure S6 in the supporting information shows the impedance spectra for

Table 2: Mean silhouette value  $\overline{s(i)}$  for the  $i^{\text{th}}$  cluster distinguished in the PCA plot of basic flavors using the whole frequency range for each IDE and the four sensing units.

IDEs	$\overline{s(1)}$	$\overline{s(2)}$	$\overline{s(3)}$	$\overline{s(4)}$	$\overline{s(5)}$	SC
IDE 1	0.89	0.89	0.88	0.85	0.91	$\overline{S(5)} = 0.88$
IDE 2	0.61	0.69	0.58	0.83	0.69	$\overline{S(5)} = 0.68$
IDE 3	0.55	0.92	0.76	0.94	0.95	$\overline{S(5)} = 0.82$
IDE 4	0.61	0.79	0.45	0.77	0.89	$\overline{S(5)} = 0.70$
All IDEs	0.85	0.94	0.82	0.88	0.91	$\overline{S(5)} = 0.88$

306 the umami-flavored food enhancer samples with the sensing units IDEs 1-4. Exposure to  
307 the food enhancers did not affect the electrical response of the sensing units, as indicated  
308 by the measurements in water in Figure S6 in the Supporting Information. The spectra  
309 are very similar to each other, in contrast to the basic flavor measurements, and distinction  
310 can only be done with a statistical analysis. The use of k-means associated with PCA  
311 allows the investigation of which sensing unit contributes most to sample distinction. The  
312 PCA plot using the whole impedance spectra for each IDE is shown in Figure S9 in the  
313 Supporting Information, while the silhouette values are given in Table 3. Full distinction of  
314 the six umami samples could be achieved using the data from a single sensing unit (IDE  
315 2, IDE 3 or IDE 4), with IDE 3 presenting the higher SC. In contrast to the analysis of  
316 basic tastes, IDE 1 (bare electrode) was unable to provide good distinction, grouping two  
317 different brands of monosodium glutamate. Therefore, there should be an optimal NP density  
318 that maximizes the distinguishing capability of a sensing unit. We also obtained SC for each  
319 cluster by combining two, three and all four IDEs, as presented in Table S2 in the Supporting  
320 Information. The highest SC was obtained by combining IDE 2, IDE 3, and IDE 4, followed  
321 by the four IDEs together. The PCA plot using the four units is shown in Figure 7, where the  
322 mean silhouette value  $\overline{s(i)}$  is higher than 0.71 for all clusters (see Table 3). Since both Ajitide  
323 IMP<sup>®</sup> and Ajitide I+G<sup>®</sup> contain disodium inosinate, they were positioned in the same  
324 region in the PC1 direction, and clearly distinguished by PC2. The latter was also useful to  
325 distinguish L-glutamic acid (also known as glutamate) from the two monosodium glutamates,  
326 i.e. Accent<sup>®</sup> and Aji-no-moto<sup>®</sup>, which were separated by PC1. The yeast extract was

327 clustered on the upper right-hand side. The distinction ability using the whole spectra  
 328 could not be improved by applying feature selection, a common procedure in information  
 329 visualization. We have tested this by applying the parallel coordinates technique<sup>56</sup> to identify  
 330 the frequencies that most contribute to the classification of the samples, but the resulting  
 331 PCA and interactive document mapping (IDMAP)<sup>56</sup> plots in Figure S10 and S11 in the  
 332 Supporting Information were not improved in comparison to Figure 7.

333 The e-tongue results taken together are a demonstration that the controlled incorporation  
 334 of nanoparticles in LbL polymer films allows for the reuse of sensing units with reproducible  
 335 electrical responses. For umami, in particular, there was no need to functionalize the sensor  
 336 surface with peptides. The high performance in distinguishing basic tastes and food en-  
 337 hancer samples with umami flavor may be exploited in monitoring other types of food and  
 338 in agriculture,<sup>57</sup> which is important to replace panels of human experts with their inherent  
 limitations due to toxicity of some compounds and personal subjectivity.<sup>58</sup>

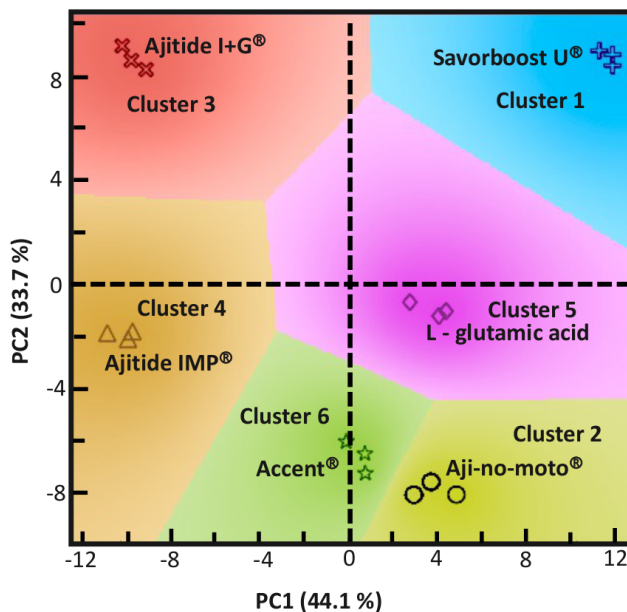


Figure 7: PCA plot obtained with the whole impedance spectra (between  $10^0$  Hz and  $10^6$  Hz) of the four sensing units of the e-tongue for the various samples having umami flavor.

339

340

Table 3: Mean silhouette values  $\overline{s(i)}$  for the  $i^{\text{th}}$  cluster distinguished in PCA for umami flavor enhancer using the whole frequency range for each IDE and the four sensing units.

IDEs	$\overline{s(1)}$	$\overline{s(2)}$	$\overline{s(3)}$	$\overline{s(4)}$	$\overline{s(5)}$	$\overline{s(6)}$	$\overline{S(k)}$
IDE 1	0.79	0.46	0.84	0.74	0.46	-	$\overline{S(5)} = 0.66$
IDE 2	0.77	0.76	0.69	0.84	0.58	0.30	$\overline{S(6)} = 0.66$
IDE 3	0.90	0.51	0.97	0.67	0.65	0.54	$\overline{S(6)} = 0.71$
IDE 4	0.98	0.21	0.91	0.90	0.87	0.32	$\overline{S(6)} = 0.70$
All IDEs	0.92	0.75	0.86	0.92	0.76	0.74	$\overline{S(6)} = 0.83$

## 341 Conclusions

342 We explored the versatility of gas-phase produced nanoparticles to modify the electrical  
343 impedance of an insulating polymer matrix by controlling the nanoparticle deposition. Impedance  
344 measurements during the nanoparticle deposition allowed us to keep track of the electrical  
345 response of IDEs covered by PAH/PSS LbL films. We also demonstrated the reproducibility  
346 and stability of the device electrical response, which supports the development of repro-  
347 ducible sensing units - a bottleneck in the field of sensing and biosensing. The sensing units  
348 were applied in an e-tongue with proof-of-principle experiments to distinguish basic tastes  
349 relevant to human perception at low molar concentrations (1 mM) and different commercial  
350 food-enhancers having the umami taste **presenting high reproducibility on triplicate analy-**  
351 **sis. The silhouette coefficient indicates better clustering in the presence of the nanoparticles**  
352 **for the umami analysis, which can also be interpreted as an increased discrimination perfor-**  
353 **mance. Briefly, the introduction of nanoparticles can be interpreted as the addition of new**  
354 **conducting pathways facilitating the electric transport and better electrode/electrolyte inter-**  
355 **action.** Our methodology to fabricate sensing units with defined impedance response opens  
356 new perspectives for monitoring food quality, in precision agriculture to evaluate nutrients  
357 in the soil and avoid over-fertilization, and the early diagnosis of many diseases. Moreover,  
358 the incorporation of nanoparticles can be extended to other types of metals and film-forming  
359 materials, thus permitting to envisage applications other than in sensing and biosensing.

## Acknowledgement

The authors are grateful to FAPESP (2007/01722-9, 2014/03691-7, 2015/14836-9, 2016/12807-4, 2017/19169-6, 2018/22214-6), CNPq, and CAPES (Finance Code 001 - 1634666/2016) for financial support. Experimental support from the Microfabrication Laboratory (proposal LMF-18748 and LMF-21855) and Electron Microscopy Laboratory (proposal TEM-21702, ME-22308, TEM-23432, TEM-24315, TEM-C1-25093) at Brazilian Nanotechnology National Laboratory (LNNano), CNPEM, Campinas, Brazil for their support with the use of equipment.

## Supporting Information Available

Dear co-authors,

The Supporting Information was submitted separately.

## References

- (1) Cichosz, S.; Masek, A.; Zaborski, M. Polymer-based sensors: A review. *Polymer Testing* **2018**, *67*, 342–348.
- (2) Montes-García, V.; Squillaci, M. A.; Diez-Castellnou, M.; Ong, Q. K.; Stellacci, F.; Samorì, P. Chemical sensing with Au and Ag nanoparticles. *Chemical Society Reviews* **2021**, *50*, 1269–1304.
- (3) Elanchezian, M.; Senthilkumar, S. Redox-active gold nanoparticle-encapsulated poly(amidoamine) dendrimer for electrochemical sensing of 4-aminophenol. *Journal of Molecular Liquids* **2021**, *325*, 115131.
- (4) Nikolaeva, N. S.; Klyamer, D. D.; Zharkov, S. M.; Tsygankova, A. R.; Sukhikh, A. S.; Morozova, N. B.; Basova, T. V. Heterostructures based on Pd–Au nanoparticles and

- 382 cobalt phthalocyanine for hydrogen chemiresistive sensors. *International Journal of*  
383 *Hydrogen Energy* **2021**, *46*, 19682–19692.
- 384 (5) Wang, F.; Hu, S. Electrochemical sensors based on metal and semiconductor nanopar-  
385 ticles. *Microchimica Acta* **2009**, *165*, 1–22.
- 386 (6) Soares, J. C.; Iwaki, L. E. O.; Soares, A. C.; Rodrigues, V. C.; Melendez, M. E.;  
387 Fregnani, J. H. T. G.; Reis, R. M.; Carvalho, A. L.; Corrêa, D. S.; Oliveira, O. N.  
388 Immunosensor for Pancreatic Cancer Based on Electrospun Nanofibers Coated with  
389 Carbon Nanotubes or Gold Nanoparticles. *ACS Omega* **2017**, *2*, 6975–6983.
- 390 (7) de Barros, A.; Constantino, C. J. L.; da Cruz, N. C.; Bortoleto, J. R. R.; Ferreira, M.;  
391 Barros, A. D.; José, C.; Constantino, L.; Cristino, N.; Roberto, J.; Bortoleto, R.;  
392 Ferreira, M. High performance of electrochemical sensors based on LbL films of gold  
393 nanoparticles, polyaniline and sodium montmorillonite clay mineral for simultaneous  
394 detection of metal ions. *Electrochimica Acta* **2017**, *235*, 700–708.
- 395 (8) Diouf, A.; Moufid, M.; Bouyahya, D.; Österlund, L.; El Bari, N.; Bouchikhi, B. An elec-  
396 trochemical sensor based on chitosan capped with gold nanoparticles combined with a  
397 voltammetric electronic tongue for quantitative aspirin detection in human physiologi-  
398 cal fluids and tablets. *Materials Science and Engineering: C* **2020**, *110*, 110665.
- 399 (9) Teodoro, K. B. R.; Shimizu, F. M.; Scagion, V. P.; Correa, D. S. Ternary nanocompos-  
400 ites based on cellulose nanowhiskers, silver nanoparticles and electrospun nanofibers:  
401 Use in an electronic tongue for heavy metal detection. *Sensors and Actuators B: Chem-*  
402 *ical* **2019**, *290*, 387–395.
- 403 (10) Garcia-Hernandez, C.; Medina-Plaza, C.; Garcia-Cabezón, C.; Blanco, Y.; Fernandez-  
404 Escudero, J. A.; Barajas-Tola, E.; Rodriguez-Perez, M. A.; Martin-Pedrosa, F.;  
405 Rodriguez-Mendez, M. L. Monitoring the Phenolic Ripening of Red Grapes Using a

- 406 Multisensor System Based on Metal-Oxide Nanoparticles. *Frontiers in Chemistry* **2018**,  
407 *6*, 131.
- 408 (11) de Sá, A. C.; Cipri, A.; González-Calabuig, A.; Stradiotto, N. R.; del Valle, M. Res-  
409 olution of galactose, glucose, xylose and mannose in sugarcane bagasse employing a  
410 voltammetric electronic tongue formed by metals oxy-hydroxide/MWCNT modified  
411 electrodes. *Sensors and Actuators B: Chemical* **2016**, *222*, 645–653.
- 412 (12) Mercante, L. A.; Scagion, V. P.; Pavinatto, A.; Sanfelice, R. C.; Mattoso, L. H. C.;  
413 Correa, D. S. Electronic tongue based on nanostructured hybrid films of gold nanopar-  
414 ticles and phthalocyanines for milk analysis. *Journal of Nanomaterials* **2015**, *2015*,  
415 24275–24281.
- 416 (13) Prakash, S.; Chakrabarty, T.; Singh, A. K.; Shahi, V. K. Polymer thin films embedded  
417 with metal nanoparticles for electrochemical biosensors applications. *Biosensors and*  
418 *Bioelectronics* **2013**, *41*, 43–53.
- 419 (14) Lin, H.; Song, L.; Huang, Y.; Cheng, Q.; Yang, Y.; Guo, Z.; Su, F.; Chen, T.  
420 Macroscopic Au@PANI Core/Shell Nanoparticle Superlattice Monolayer Film with  
421 Dual-Responsive Plasmonic Switches. *ACS Applied Materials and Interfaces* **2020**, *12*,  
422 11296–11304.
- 423 (15) Maréchal, N.; Quesnel, E.; Pauleau, Y. Silver thin films deposited by magnetron sput-  
424 tering. *Thin Solid Films* **1994**, *241*, 34–38.
- 425 (16) Chan, K. Y.; Teo, B. S. Sputtering power and deposition pressure effects on the electrical  
426 and structural properties of copper thin films. *Journal of Materials Science* **2005**, *40*,  
427 5971–5981.
- 428 (17) Arnalds, U. B.; Agustsson, J. S.; Ingason, A. S.; Eriksson, A. K.; Gylfason, K. B.;  
429 Gudmundsson, J. T.; Olafsson, S. A magnetron sputtering system for the preparation

- 430 of patterned thin films and in situ thin film electrical resistance measurements. *Review*  
431 *of Scientific Instruments* **2007**, *78*, 1–6.
- 432 (18) Novotny, M. In-situ monitoring of the growth of nanostructured aluminum thin film.  
433 *Journal of Nanophotonics* **2011**, *5*, 051503.
- 434 (19) Abdellaoui, N.; Pereira, A.; Novotny, M.; Bulir, J.; Fitl, P.; Lancok, J.; Moine, B.;  
435 Pillonnet, A. In situ monitoring of electrical resistance during deposition of Ag and  
436 Al thin films by pulsed laser deposition: Comparative study. *Applied Surface Science*  
437 **2017**, *418*, 517–521.
- 438 (20) Haberland, H.; Karrais, M.; Mall, M.; Thurner, Y. Thin films from energetic cluster  
439 impact: A feasibility study. *Journal of Vacuum Science & Technology A: Vacuum,*  
440 *Surfaces, and Films* **1992**, *10*, 3266–3271.
- 441 (21) Wegner, K.; Piseri, P.; Tafreshi, H. V.; Milani, P. Cluster beam deposition: a tool for  
442 nanoscale science and technology. *Journal of Physics D: Applied Physics* **2006**, *39*,  
443 R439–R459.
- 444 (22) Arrieta, A.; Rodriguez-Mendez, M. L.; de Saja, J. A. Langmuir–Blodgett film and  
445 carbon paste electrodes based on phthalocyanines as sensing units for taste. *Sensors*  
446 *and Actuators B: Chemical* **2003**, *95*, 357–365.
- 447 (23) Ferreira, M.; Riul Antonio,; Wohnrath, K.; Fonseca, F. J.; Oliveira Osvaldo N.,; Mat-  
448 toso, L. H. C. High-Performance Taste Sensor Made from Langmuir-Blodgett Films  
449 of Conducting Polymers and a Ruthenium Complex. *Analytical Chemistry* **2003**, *75*,  
450 953–955.
- 451 (24) Lvova, L.; Pudi, R.; Galloni, P.; Lippolis, V.; Di Natale, C.; Lundström, I.; Paolesse, R.  
452 Multi-transduction sensing films for Electronic Tongue applications. *Sensors and Ac-*  
453 *tuator B: Chemical* **2015**, *207*, 1076–1086.

- 454 (25) Daikuzono, C. M.; Dantas, C. A.; Volpati, D.; Constantino, C. J.; Piazzetta, M. H.;  
455 Gobbi, A. L.; Taylor, D. M.; Oliveira, O. N.; Riul, A. Microfluidic electronic tongue.  
456 *Sensors and Actuators, B: Chemical* **2015**, *207*, 1129–1135.
- 457 (26) Toko, K. Taste sensor with global selectivity. *Materials Science and Engineering: C*  
458 **1996**, *4*, 69–82.
- 459 (27) Toko, K. Taste sensor. *Sensors and Actuators B: Chemical* **2000**, *64*, 205–215.
- 460 (28) Decher, G.; Hong, J.; Schmitt, J. Buildup of ultrathin multilayer films by a self-assembly  
461 process: III. Consecutively alternating adsorption of anionic and cationic polyelec-  
462 trolytes on charged surfaces. *Thin Solid Films* **1992**, *210-211*, 831–835.
- 463 (29) Decher, G. *Multilayer Thin Films*; Wiley Online Books; 2012; pp 1–21.
- 464 (30) Hensel, R. C.; Rodrigues, K. L.; Pimentel, V. D. L.; Riul, A.; Rodrigues, V. Automated  
465 self-assembly and electrical characterization of nanostructured films. *MRS Communi-*  
466 *cations* **2018**, *8*, 283–288.
- 467 (31) Hensel, R. C.; Pereira-da Silva, M. A.; Riul, A.; Rodrigues, V. Dielectric Permittivity  
468 and Surface Charge Density in Layer-by-Layer Poly(diallyldimethylammonium chlo-  
469 ride)/Poly(styrenesulfonate) Nanostructured Films: Implications for Biosensing. *ACS*  
470 *Applied Nano Materials* **2020**, *3*, 1749–1754.
- 471 (32) de Sá, A. D. T.; Abrao Oiko, V. T.; di Domenicantonio, G.; Rodrigues, V. New exper-  
472 imental setup for metallic clusters production based on hollow cylindrical magnetron  
473 sputtering. *Journal of Vacuum Science & Technology B, Nanotechnology and Micro-*  
474 *electronics: Materials, Processing, Measurement, and Phenomena* **2014**, *32*, 061804.
- 475 (33) Hensel, R. C.; Gonçalves, M. H.; Rodrigues, K. L.; A. Oiko, V. T.; do L. Pimentel, V.;  
476 Pereira-da Silva, M. A.; Hillenkamp, M.; Riul Jr., A.; Rodrigues, V. Monitoring and

- 477 modeling the deposition of metal nanoparticles on surfaces by impedance. *Applied Sur-*  
478 *face Science* **2020**, 148806.
- 479 (34) Rivera, F.; Davis, R.; Vanfleet, R. Alternative FIB TEM sample preparation method  
480 for cross-sections of thin metal films deposited on polymer substrates. *Microscopy and*  
481 *Microanalysis* **2013**, *19*, 1080–1091.
- 482 (35) Shimizu, F. M.; Braunger, M. L.; Riul Jr., A.; Oliveira Jr., O. N. Electronic Tongues.  
483 2020; <https://doi.org/10.1002/9781119587422.ch4>.
- 484 (36) Garçon, L. A.; Genua, M.; Hou, Y.; Buhot, A.; Calemczuk, R.; Livache, T.; Billon, M.;  
485 Narvor, C. L.; Bonnaffé, D.; Lortat-Jacob, H.; Hou, Y. A versatile electronic tongue  
486 based on surface plasmon resonance imaging and cross-reactive sensor arrays—a mini-  
487 review. *Sensors (Switzerland)* **2017**, *17*, 1–12.
- 488 (37) Taylor, D.; Macdonald, A. AC admittance of the metal/insulator/electrolyte interface.  
489 *Journal of Physics D: Applied Physics* **1987**, *20*, 1277.
- 490 (38) Inc., S. A. ZView® For Windows. 2017; [https://www.scribner.com/software/](https://www.scribner.com/software/68-general-electrochemistr376-zview-for-windows/)  
491 [68-general-electrochemistr376-zview-for-windows/](https://www.scribner.com/software/68-general-electrochemistr376-zview-for-windows/).
- 492 (39) Macdonald, J. R.; Barsoukov, E. Impedance spectroscopy: theory, experiment, and  
493 applications. *History* **2005**, *1*, 1–13.
- 494 (40) Davies, H. M.; Hope, K. Methods of Multivariate Analysis. *The Mathematical Gazette*  
495 **1972**, *56*.
- 496 (41) Orange Website. 2019; [www.orange.com](http://www.orange.com), visited on 2020-11-11.
- 497 (42) Hartigan, J. A.; Wong, M. A. A K-Means Clustering Algorithm. *Journal of the Royal*  
498 *Statistical Society: Series C (Applied Statistics)* **1979**, *28*, 100–108.
- 499 (43) Kaufman, L.; Rousseeuw, P. J. *Eepe.Ethz.Ch*; 1990.

- 500 (44) Struyf, A.; Hubert, M.; Rousseeuw, P. Clustering in an Object-Oriented Environment.  
501 *Journal of Statistical Software, Articles* **1997**, *1*, 1–30.
- 502 (45) Braunger, M. L.; Fier, I.; Rodrigues, V.; Arratia, P. E.; Riul, A. Microfluidic Mixer  
503 with Automated Electrode Switching for Sensing Applications. *Chemosensors* **2020**, *8*,  
504 13.
- 505 (46) Yang, Y.; Chen, Q.; Shen, C.; Zhang, S.; Gan, Z.; Hu, R.; Zhao, J.; Ni, Y. Evaluation of  
506 monosodium glutamate, disodium inosinate and guanylate umami taste by an electronic  
507 tongue. *Journal of Food Engineering* **2013**, *116*, 627–632.
- 508 (47) Feng, T.; Bing, F.; Yang, Y.; Zhuang, H.; Ye, R.; Li, X.; Xu, Z.; Wang, K. Discrim-  
509 ination of edible fungi varieties and evaluation of their umami intensities by using an  
510 electronic tongue method. *International Journal of Food Science & Technology* **2016**,  
511 *51*, 1393–1400.
- 512 (48) Phat, C.; Moon, B.; Lee, C. Evaluation of umami taste in mushroom extracts by  
513 chemical analysis, sensory evaluation, and an electronic tongue system. *Food Chemistry*  
514 **2016**, *192*, 1068–1077.
- 515 (49) Mondal, D.; Paul, D.; Mukherji, S. Conducting polymer coated filter paper based dis-  
516 posable electronic tongue. 2018 12th International Conference on Sensing Technology  
517 (ICST). 2018; pp 7–12.
- 518 (50) Ahn, S. R.; An, J. H.; Jang, I. H.; Na, W.; Yang, H.; Cho, K. H.; Lee, S. H.; Song, H. S.;  
519 Jang, J.; Park, T. H. High-performance bioelectronic tongue using ligand binding do-  
520 main T1R1 VFT for umami taste detection. *Biosensors and Bioelectronics* **2018**, *117*,  
521 628–636.
- 522 (51) Wei, X.; Qin, C.; Gu, C.; He, C.; Yuan, Q.; Liu, M.; Zhuang, L.; Wan, H.; Wang, P. A  
523 novel bionic in vitro bioelectronic tongue based on cardiomyocytes and microelectrode  
524 array for bitter and umami detection. *Biosensors and Bioelectronics* **2019**, *145*, 111673.

- 525 (52) Dang, Y.; Hao, L.; Zhou, T.; Cao, J.; Sun, Y.; Pan, D. Establishment of new assessment  
526 method for the synergistic effect between umami peptides and monosodium glutamate  
527 using electronic tongue. *Food Research International* **2019**, *121*, 20–27.
- 528 (53) Wang, W.; Zhou, X.; Liu, Y. Characterization and evaluation of umami taste: A review.  
529 *TrAC Trends in Analytical Chemistry* **2020**, *127*, 115876.
- 530 (54) Hwang, Y.-H.; Ismail, I.; Joo, S.-T. Identification of Umami Taste in Sous-Vide Beef by  
531 Chemical Analyses, Equivalent Umami Concentration, and Electronic Tongue System.  
532 **2020**, *9*.
- 533 (55) Fukushima, K. L.; Scagion, V. P.; Facure, M. H. M.; Pinheiro, A. C. M.; Correa, D. S.;  
534 Nunes, C. A.; Oliveira, J. E. Development of an Electronic Tongue Based on a Nanocom-  
535 posite for Discriminating Flavor Enhancers and Commercial Salts. *IEEE Sensors Jour-*  
536 *nal* **2021**, *21*, 1250–1256.
- 537 (56) Paulovich, F. V.; Moraes, M. L.; Maki, R. M.; Ferreira, M.; Oliveira Jr., O. N.;  
538 de Oliveira, M. C. F. Information visualization techniques for sensing and biosensing.  
539 *Analyst* **2011**, *136*, 1344–1350.
- 540 (57) Srivastava, A. K.; Dev, A.; Karmakar, S. Nanosensors and nanobiosensors in food and  
541 agriculture. *Environmental Chemistry Letters* **2018**, *16*, 161–182.
- 542 (58) Smyth, H.; Cozzolino, D. Instrumental Methods (Spectroscopy, Electronic Nose, and  
543 Tongue) As Tools To Predict Taste and Aroma in Beverages: Advantages and Limita-  
544 tions. *Chemical Reviews* **2013**, *113*, 1429–1440.

## 545 Graphical TOC Entry

546

Some journals require a graphical entry for the Table of Contents. This should be laid out “print ready” so that the sizing of the text is correct.

Inside the tocentry environment, the font used is Helvetica 8 pt, as required by *Journal of the American Chemical Society*.

The surrounding frame is 9 cm by 3.5 cm, which is the maximum permitted for *Journal of the American Chemical Society* graphical table of content entries. The box will not resize if the content is too big: instead it will overflow the edge of the box.

This box and the associated title will always be printed on a separate page at the end of the document.